Published in final edited form as:
Nat Geosci. 2019 June 27; 12(8): 667–671. doi:10.1038/s41561-019-0411-x.

Arc magmas oxidised by water dissociation and hydrogen incorporation in orthopyroxene

Peter Tollan[1] **Jörg Hermann**[1]

[1]Institut für Geologie, University of Bern, Switzerland

Abstract

Elevated H_2O concentrations and oxygen fugacities are two fundamental properties that distinguish magmas formed in subduction zones from new crust generated at mid ocean ridges. However, the mechanism of magma oxidation, and how it relates to the increase in H_2O remains unclear. In this study, we use infrared spectroscopy of mantle wedge orthopyroxene to trace the temporal and spatial evolution of oxygen fugacity during transport of hydrous arc melts towards the crust. A positive correlation between equilibrium oxygen fugacity and orthopyroxene H_2O concentrations for the peridotite samples studied allowed the assignment of specific, commonly-observed absorption bands to redox-sensitive crystallographic defects. H_2O content associated with these redox-sensitive defects increases in concentration across individual crystals, uniquely preserving the time-dependent transition from reduced to oxidised conditions during the migration of hydrous melts through the mantle wedge. A separate, but related process of reaction with H_2 occurring primarily during the earliest stages of melt-mantle reaction may be fundamental in generating the oxidised nature of hydrous melts. Our study proposes that the oxidised nature of arc magmas may not be a primary feature, but is instead acquired progressively as hydrous primary melts react with the surrounding mantle.

High water concentrations and oxidised conditions significantly modify the crystallisation sequence in arc magmas[3,4], and are consequently an important reason for the bimodal distribution of terrestrial crustal compositions[5]. Despite the apparent association of H_2O and fO_2, it is unclear to what extent these properties are dependent on each other. The oxidation state of arc magmas is evident in their higher average Fe valence state (Fe^{3+}/Fe^{2+}) compared to mid-ocean ridge basalts[1] (MORB). Correlations between oxidation state, water, and trace element and isotope ratios characteristic of slab-derived fluids have led to the conventional view that the high fO_2 of arc melts are derived externally during fluid-enabled melting in the

Author contributions
P.M.E.T designed and conducted the FTIR measurements, and processed the data. P.M.E.T and J.H interpreted the data and wrote the manuscript.

Competing interests
The authors declare no competing interests

Data availability
All supporting data for the manuscript are provided as a supplementary file. Any additional data may be requested from the authors.

Europe PMC Funders Author Manuscripts

mantle[1,6,7] (Fig. 1). This hypothesis is, however, inconsistent with the concentrations of redox-sensitive incompatible major and trace elements in primitive arc basalts, which, when normalised to redox-insensitive elements of similar compatibility, are indistinguishable from MORB[8–10]. As a result, alternative models for melt oxidation have been proposed, focusing on aspects of crustal differentiation, particularly crystal fractionation and degassing[9,11–13]. As yet, none of these mechanisms have reached a level of consensus in the geological community[12,14]. Here we provide evidence from Fourier transform infrared (FTIR) spectroscopy of mantle wedge orthopyroxene that demonstrates that arc melts are already oxidised before crustal differentiation. We then use this data to support a mechanism, which can resolve the discrepancy between current models of arc magma oxidation.

Peridotite xenolith textures and equilibration conditions

The samples studied are mantle harzburgite xenoliths recovered from seamounts surrounding Ritter island, part of the active West Bismarck island arc. Previous studies identified two distinct groups, based on their texture, geochemistry and petrogenetic interpretation[15–17]. The first group represents the ambient mantle. They display a well-equilibrated protogranular texture, low equilibration temperatures (<700-800 °C), and highly depleted major and trace element mineral compositions, interpreted to reflect high degrees of hydrous melting in a previous subduction zone setting, followed by sub-solidus cooling[16]. Pressure is best constrained by the low equilibration temperature of these protogranular peridotites and the absence of plagioclase or garnet. Based on a typical arc geotherm[18], pressure estimates of 1.2-1.5 GPa are appropriate for this sample suite. The studied samples thus derive from the uppermost part of the mantle wedge[16]. The second group contains evidence for modification of this original texture through reaction with arc melts within the modern day mantle wedge (Fig. 1), prior to their entrainment and eruption as xenoliths in the host lava[15]. These reaction textures vary considerably both in their physical nature and their occurrence, but typically take the form of veins or patches of secondary orthopyroxene (± clinopyroxene and glass), formed at the expense of olivine[16]. Geochemical features associated with these textures include varying degrees of major and trace element modification of the pre-existing phases, reflected in higher equilibration temperatures (900-1200 °C)[15–17]. The fO_2 of the protogranular, ambient mantle samples spans a wide range, from reduced (0.8 log units below the fayalite-magnetite-quartz (FMQ) buffer) to moderately oxidised (Δlog FMQ +0.2)[17]. The samples bearing textural evidence for melt-rock reaction have the most oxidised compositions (Δlog FMQ +1.0-1.5), indicating that the range in fO_2 of the sample suite is controlled by the proximity of the reduced ambient mantle to oxidised percolating melt channels (Fig. 1). The oxidised nature of primary mantle melts is supported by a previous assessment of the host basalt fO_2 based on olivine-melt V partitioning, which yielded a value of Δlog FMQ +2.2[15].

Relationships between infrared spectra and fO_2

A subset of Ritter harzburgites was selected for measurements of H_2O concentration by FTIR. Samples were selected to encompass a broad range of fO_2 (-0.8 to +1.0 Δlog FMQ[17]) and temperature (~700-1000 °C[16,17]) so that the H_2O concentrations and incorporation mechanisms could be assessed as a function of these key parameters. Of the two primary

minerals present, orthopyroxene is of particular interest, since it is the dominant host of H in the depleted upper mantle, and the slower rate of H diffusion compared to olivine means the concentrations are less likely to be modified during magmatic ascent[19–22]. Average FTIR spectra were acquired using the cores of multiple residual orthopyroxenes per sample, and subsequently deconvoluted into their constitutive absorption bands, located at 3600 cm^{-1}, 3544 cm^{-1}, 3520 cm^{-1}, 3420-3390 cm^{-1}, 3320 cm^{-1} and 3060 cm^{-1} (Fig. 2). Comparison with global data for mantle orthopyroxene reveals that two of these bands (~3520 cm^{-1} and ~3420 cm^{-1}) are ubiquitous. Bands between 3600-3590 cm^{-1} are present in nearly 90% of published spectra, whilst bands at 3320-3300 cm^{-1} and 3075-3060 cm^{-1} are observed in more than half (Supplementary Fig. 1). Note that the presence of other secondary phases (glass and clinopyroxene) within secondary orthopyroxene veins and patches[16] prevented FTIR measurement of secondary orthopyroxene in reacted samples.

There is a positive correlation ($R^2 = 0.80$) between the average H_2O concentrations of orthopyroxene cores (31-92 wt. ppm) and fO_2 (Supplementary Fig. 7), with the two samples with reaction textures having the highest H_2O and fO_2. There is no correlation between H_2O and Al_2O_3 (Supplementary Fig. 7), however the very low Al_2O_3 concentrations of the orthopyroxenes (1.2-1.7 wt.%) is likely a governing factor in the low overall H_2O concentrations compared to the global mantle range (0 to ~400 ppm)[19,20]. Comparing the integrated absorption of individual bands shows highly variable behaviour (Fig. 2). Bands with substantial differences in intensity between samples (3544 and 3520 cm^{-1}, 3320 cm^{-1} and 3060 cm^{-1}) correlate strongly ($R^2 = 0.87$-0.93) with fO_2, whereas others do not (3600 cm^{-1} and 3420-3395 cm^{-1}). Based on this disparate behaviour we are able, for the first time, to link specific infrared bands in natural orthopyroxene with a physical parameter. The redox-sensitive bands are interpreted to reflect coupling of H with a heterovalent cation, most likely Fe, which has a valence state of +2 or +3 depending on the fO_2 (see Supplementary Information for details of the incorporation reactions). While Cr can also occur in both +2 and +3 valence states, over the range of fO_2 of the samples the bulk valence is expected to be constant and hence Cr is not a plausible candidate for generating the relationship with fO_2[22]. The lack of correlation between the remaining bands and any element or intensive variable means that it is most likely that they reflect hydrated Si vacancies, consistent with experimental studies[24]. We rule out the role of temperature in contributing significantly to the infrared band variations, since an increase in temperature is unlikely to generate distinctly new hydrous defects. We note that band-defect assignments have also been made for experimental samples, however the bands generated in these experiments tend to differ significantly compared to natural samples[22,24].

To further constrain the origin of the relationships between H_2O and fO_2, high-resolution (5.4-10.8 μm scale) FTIR maps and profiles were made of orthopyroxene crystals from each sample (Fig. 3 and Supplementary Fig. 3-4). Most of the samples demonstrate equilibrium with the ambient mantle conditions for H_2O, represented by relatively flat core concentrations. Occasionally, H-loss profiles towards the crystal rims are observed, most likely in response to a decrease in host magma fH_2O during ascent[15]. One protogranular sample (67-02 B(1)[16], Fig. 2), however, uniquely captures the transition between reduced, dry ambient mantle and oxidised, wet reacted mantle (Fig. 3, Supplementary Fig. 3-4). Total integrated absorption across orthopyroxenes from this sample increases substantially from

Europe PMC Funders Author Manuscripts

crystal cores to rims, overprinted by a small decrease in the outermost 50 μm. Deconvoluting the total absorbance into the individual bands as before reveals variable behaviour for redox-sensitive and redox-insensitive bands. Redox-sensitive bands show up to an order of magnitude increase from core to rim (typically a factor of 2-5 depending on the band and crystal) with a small decrease at the rim. While a previous study of an end-member, highly melt-reacted peridotite shows H_2O incorporation mediated by coupled substitution with other diffusing trace elements[15], the mechanism of H_2O incorporation in the samples studied here is different. Major element profiles along the crystals containing H_2O zoning are essentially homogeneous (Supplementary Fig. 6) and the bulk rock texture and mineral chemistry is indistinguishable from other protogranular, ambient mantle samples[16,17]. Hence, H_2O incorporation is independent of bulk chemical changes in the crystals, within the limits of detection. In contrast, redox-insensitive bands show more typical diffusive loss profiles, with approximately homogeneous concentrations towards the core and more pronounced H-loss at the rim. It is important to emphasise that, although H in orthopyroxene is in the structural form of hydroxyl (O-H), it can be acquired from different H-bearing species in the fluid phase: H_2 and H_2O. Reaction of orthopyroxene with H_2, however, requires reduction of Fe^{3+}, which should result in an opposite trend with fO_2 to that observed here[19,22]. Therefore, the mechanism responsible involves a reaction involving H_2O, which leads to a simultaneous increase in the Fe^{3+}/Fe^{2+} ratio in orthopyroxene (see Supplementary Information).

How H_2O incorporation in orthopyroxene monitors fO_2

The first-order conclusion that can be drawn from this dataset is that hydrous arc melts must already be oxidised by the time they reach the upper mantle wedge. The relative intensities of redox-sensitive and redox-insensitive infrared bands described here provide a novel method of monitoring mantle fO_2, although application to other sample suites would require the effect of pressure on infrared band behaviour to be taken into acount[22]. The range of textures present in the Ritter suite[15–17], and the gradients observed in equilibration conditions implies that modification by melt-rock reaction is gradational depending on proximity to the melt (Fig. 1) or, analogously, to the timescale of melt-rock reaction for a given distance from a melt channel. Immediately at the point of reaction, modal metasomatic changes to the peridotite composition occur (namely the formation of secondary mineral veins), which show H_2O incorporation mediated by bulk chemical modification[15]. In a spatially limited zone surrounding the melt channel, the bulk chemistry and texture of the ambient mantle remain unmodified, but mineral chemistry will progressively re-equilibrate with the temperature and fO_2 of the melt through electron exchange and inter-mineral diffusion of temperature-sensitive components (dependent on the kinetics of the diffusing components). Concurrently, H_2O rapidly diffuses into the mantle along grain boundaries[25], followed by incorporation into orthopyroxene mediated by the elevated fO_2 (see Supplementary Information).

The increasing concentrations of redox-sensitive hydrous point defects across single orthopyroxene crystals provide temporal information on the changes in fO_2 and H_2O content of the mantle wedge, demonstrating that both of these properties are modified rapidly from their reduced and dry ambient mantle conditions. To place a more precise constraint on the

timescale for this process, the diffusion of H associated with redox-sensitive bands was modelled (see Supplementary Information for detailed explanation and figures). Assuming a temperature of H diffusion similar to the average temperature of samples with reaction textures, the transformation of reduced to oxidised mantle occurred over a period of ~1 month. We suggest therefore that the range of fO_2 and associated H_2O in orthopyroxene in the Ritter samples reflects distance from percolating melts induced relatively recently in their petrogenesis, rather than more long-term properties of the mantle wedge inherited prior[17]. A clear distinction must be made between the timescales of this incorporation process, which operated in the mantle, and the later loss of hydrogen triggered during eruption of the xenoliths, evidenced by the outermost tens of μm at the orthopyroxene rims. The former occurred on timescales of months, whilst xenolith exhumation was considerably quicker (several hours)[15]. The data reported here show that while orthopyroxene H_2O contents can be modified during ascent, similarly to olivine, the rate of H diffusion is slow enough to preserve significant information pertaining to mantle processes.

A model for hydrous melt oxidation

Finally, we propose that the interaction of the mantle wedge with passing hydrous melts might also provide new information on the relationship between elevated water contents and the oxidised nature of arc magmas. It has been previously suggested that dissociation of H_2O in mantle fluids, followed by incorporation of H in mantle olivine by reaction with H_2, mediated by reduction of ferric to ferrous iron, may be a viable mechanism for oxidising hydrous mantle fluids[26–28]. Instead, we propose a key role for orthopyroxene due to its greater H_2O storage capacity and higher amounts of ferric iron compared to olivine. The model we propose for melt oxidation is as follows: hydrous mantle melts and the ambient mantle wedge have an initial fO_2 similar to MORB (~FMQ -1), consistent with the Sc-V and Fe-Zn systematics of primitive arc basalts[8–10]. During the earliest stages of melt ascent and reaction with the mantle, H_2 is lost from the melt and incorporated in surrounding orthopyroxene and, to a lesser extent, olivine and clinopyroxene (mechanism 1 in Fig 1 and equilibria 2 and 3 in the Supplementary Information). This H_2-loss is driven by the large gradient in fH_2 between the highly depleted ambient mantle wedge and the hydrous melt, and accomplished by the rapid rates of H diffusion (both along grain boundaries and through mineral lattices[25]). This early stage of reaction with H_2 results in a net oxidation of the melt and corresponding reduction of the mantle[19,28]. Assuming a FeO^{total} content of 8 wt.% and an initially reducing condition reflected by an Fe^{3+}/Fe^{tot} of 0.1 (typical of MORB[1]) the dissociation of only 0.2 wt.% H_2O would be required in order to modify this mean Fe valence state to a more oxidised ratio of 0.3, typical of oxidised arc basalts[1] (see full mass balance in Supplementary Information). This mechanism would produce a trend of increasing H_2O in orthopyroxene with decreasing fO_2, as has been observed both experimentally[22] and in other arc mantle peridotite samples[19]. Evidence for this mechanism may be present in the most reduced Ritter peridotites (i.e., furthest from the oxidising influence of the melt channel), which still have ~30 ppm H_2O, considerably more than would be anticipated given the highly depleted nature of the mantle[16]. As the increasingly oxidised melts ascend through the mantle wedge, the local mantle adjacent to the melt channels becomes progressively oxidised, leading to H_2O incorporation by mechanism 2

(Fig 1 and equilibria 4 and 5 in the Supplementary Information). This second mechanism does not significantly modify further the fO_2 of the melt, but instead acts as a sensor for the evolving fO_2 of the melt-peridotite system. The first mechanism involving reaction with H_2 is still likely to happen at these shallow levels of the upper mantle, but only in regions further from the melt channel which are not influenced by the oxidising effect of intruding melt (but still accessible to H_2 due to its rapid diffusivity[25]). If this model of melt oxidation and sensing operate to the extent suggested here then it would reconcile the apparently contradictory evidence for the origin of the oxidised nature of arc magmas.

Methods

Temperature and fO_2

Values of equilibrium fO_2 and temperature of six of the seven samples reported here were taken from ref. 17, which utilised Mössbauer spectroscopy to directly measure Fe^{3+}/Fe^{2+} ratios in spinel (or alternatively employed Mössbauer-calibrated spinel standards to correct estimates of Fe^{3+}/Fe^{2+} by electron microprobe). The remaining two samples were not included in ref. 17, however electron microprobe data for all constituent phases was reported by ref. 16. Since neither Mössbauer spectroscopy nor Mössbauer-calibrated standards were used in this study, the estimates of spinel Fe^{3+}/Fe^{2+} from the electron microprobe data were corrected to match the more reliable data of ref. 17. This was done by plotting the calculated fO_2 of three samples measured by both studies (Supplementary Fig. 5). This revealed an average offset of 0.39 log units, and hence the fO_2 of the remaining samples were increased by this amount from the value calculated using the raw data of ref. 16. Uncertainty in fO_2 was taken from ref. 17, however uncertainty in temperature is unrealistically low, and hence was recalculated from the standard deviation of mineral compositions for the same samples reported by ref. 16.

FTIR spectroscopy

Water contents of orthopyroxene were determined by Fourier transform infrared spectroscopy at the Institut für Geologie, Universität Bern, Switzerland. Peridotite samples were cut into sections approximately 400 μm thick and then polished on both sides to 1 μm grade. Multiple (8-20) orthopyroxene grains were selected from each sample for *in-situ* FTIR analysis. Measurements were conducted in transmission mode and unpolarised light using a Bruker Tensor II spectrometer with a globar infrared source and a KBr beamsplitter, coupled to a Bruker Hyperion 3000 microscope with a dry air-purged sample chamber. The cores of each crystal were measured using a liquid nitrogen-cooled mercury cadmium telluride (MCT) detector, employing a ~50x50 μm square spot, 64 scans and 4 cm^{-1} resolution. High resolution maps were acquired from selected grains using a liquid nitrogen-cooled focal plane array (FPA) detector, which consists of 4096 detector elements arranged over a measurement grid with fixed dimensions of approximately 170x170 μm to give a nominal resolution of ~2.7 μm. Since the numerical aperture of the 15x objective provided by Bruker is 0.4, the theoretical resolution limit in the water stretching region of orthopyroxene (~2800-3700 cm^{-1}) is 5.4-4.1 μm (according to the relationship $\Delta x = 0.61(\lambda/NA)$, where Δx is distance, λ is infrared wavelength in air and NA is numerical aperture). Thus, the raw data was binned, with final resolutions of 5.4 μm or 10.8 μm, depending on

grain size. Profiles were constructed by extracting 5 perpendicular lines across the FPA maps and then averaging the data at each pixel step, producing a pseudo rectangular spot of either 5.4x27 μm or 10.8x54 μm, depending on the original map resolution. Both MCT and FPA data were processed using the OPUS software provided by Bruker. Data were corrected for atmospheric contamination using the algorithm built into OPUS, and then baseline-corrected using the "concave rubberband" algorithm (3 iterations and 64 baseline points). Of the two samples bearing reaction textures, one (67-02A(5)) had significant contamination of many orthopyroxene spectra by melt/fluid inclusions introduced during melt-rock reaction, and epoxy introduced during sample preparation. These manifested as numerous intense bands located at 2760-3000 cm^{-1} (epoxy) and a single broad, intense band at 3150-3650 cm^{-1}. Spectra included in the calculations presented in this study were carefully selected to minimise the contribution of such contaminants. Thickness of the grains was measured using a digital micrometer with a precision of ~3 μm. Profiles across crystals were inspected for thickness variations by monitoring the absorbance of the overtone and combination bands (1200-2200 cm^{-1}). Total water concentrations were calculated from the average integrated absorbance (~2800-3700 cm^{-1}) of multiple orthopyroxene cores from each sample using the method of ref. 29 and ref. 30, recently developed further by ref 31. An integrated molar absorption coefficient of 14.84 ppm^{-1} cm^{-2} was used to convert the average integrated absorbance into ppm H_2O[32]. In order to determine the contribution of individual bands to the total integrated absorbance, all spectra were deconvoluted using a linear least squares approach and assuming band shapes which were linear mixtures of Gaussian and Lorentzian functions (pseudo-Voigt).

Supplementary Material

Refer to Web version on PubMed Central for supplementary material.

Acknowledgments

Richard Arculus is thanked for providing the samples. Daniela Rubatto and Michael Jollands are thanked for discussions and feedback. This work was supported by the SNF project: 200021_169062.

References

1. Kelley KA, Cottrell E. Water and the Oxidation State of Subduction Zone Magmas. Science. 2009; 325:605–607. [PubMed: 19644118]
2. Frost DJ, McCammon CA. The redox state of Earth's mantle. Annu Rev Earth Planet Sci. 2008; 36:389–420.
3. Osborn EF. Role of oxygen pressure in the crystallization and differentiation of basaltic magma. Am J Science. 1959; 257:609–647.
4. Sisson TW, Grove TL. Experimental investigations of the role of H_2O in calc-alkaline differentiation and subduction zone magmatism. Contrib Mineral Petrol. 1993; 113:143–166.
5. Campbell IH, Taylor SR. No water, no granites – no oceans, no continents. Geophys Res Lett. 1983; 10:1061–1064.
6. Pons M-L, Debret B, Bouilhol P, Delacour A, Williams H. Zinc isotope evidence for sulfate-rich fluid transfer across subduction zones. Nature Comm. 2016; 7:13794.
7. Bénard A, et al. Oxidising agents in sub-arc mantle melts link slab devolatilisation and arc magmas. Nature Comm. 2018; 9:3500.

8. Lee C-TA, Leeman WP, Canil D, Li Z-XA. Similar V/Sc systematics in MORB and arc basalts: implications for the oxygen fugacities of their mantle source regions. J Petrol. 2005; 46:2313–2336.
9. Lee C-TA, Luffi P, Le Roux V, Dasgupta R, Albaréde F, Leeman WP. The redox state of arc mantle using Zn/Fe systematics. Nature. 2010; 468:681–685. [PubMed: 21124454]
10. Mallmann G, O'Neill HStC. The crystal/melt partitioning of V during mantle melting as a fuction of oxygen fugacity compared with some other elements (Al, P, Ca, Sc, Ti, Cr, Fe, Ga, Y, Zr and Nb). J Petrol. 2009; 50:1765–1794.
11. Burgisser A, Scaillet B. Redox evolution of a degassing magma rising to the surface. Nature. 2007; 445:194–197. [PubMed: 17215841]
12. Humphreys MCS, et al. Coupled interactions between volatile activity and Fe oxidation state during arc crustal processes. J Petrol. 2015; 56:795–814.
13. Lee C-TA. et al. Copper systematics in arc magmas and implications for crust-cantle differentiation. Science. 2012; 336:64–68. [PubMed: 22491850]
14. Waters LE, Lange RA. No effect of H_2O degassing on the oxidation state of magmatic liquids. Earth Planet Sci Lett. 2016; 447:48–59.
15. Tollan PME, O'Neill HStC, Hermann J, Benedictus A, Arculus RJ. Frozen melt-rock reaction in a peridotite xenolith from sub-arc mantle recorded by diffusion of trace elements and water in olivine. Earth Planet Sci Lett. 2015; 422:169–181.
16. Tollan PME, Dale CW, Hermann J, Davidson JP, Arculus RJ. Generation and modification of the mantle wedge and lithosphere beneath the west bismarck island arc: melting, metasomatism and thermal history of peridotite xenoliths from Ritter island. J Petrol. 2017; 58:1475–1510.
17. Bénard A, Woodland AB, Arculus RJ, Nebel O, McAlpine SRB. Variation in sub-arc mantle oxygen fugacity during partial melting recorded in refractory peridotite xenoliths from the West Bismarck Arc. Chemical Geology. 2018; 486:16–30.
18. Wada I, Wang K. Common depth of slab-mantle decoupling: Reconciling diversity and uniformity of subduction zones. Geochem Geophys Geosys. 2009; 10doi: 10.1029/2009GC002570
19. Peslier AH, Luhr JF, Post J. Low water contents in pyroxenes from spinel-peridotites of the oxidized, sub-arc mantle wedge. Earth Planet Sci Lett. 2002; 201:69–86.
20. Demouchy S, Bolfan-Casanova N. Distribution and transport of hydrogen in the lithospheric mantle: A review. Lithos. 2016; 240-243:402–425.
21. Tian Z-ZT, et al. Water concentration profiles in natural mantle orthopyroxenes: A geochronometer for long annealing of xenoliths within magma. Geology. 2017; 45:87–90.
22. Stalder R, Skogby H. Dehydration mechanisms in synthetic Fe-bearing enstatite. Eur J Mineral. 2007; 19:201–216.
23. Karner JM, et al. Valence state partitioning of Cr between pyroxene-melt: Effects of pyroxene and melt compositions and direct determination of Cr valence states by XANES. Application to Martian basalt QUE 94201 composition. Am Mineral. 2007; 92:2002–2005.
24. Prechtel F, Stalder R. OH-defects in Al- and Cr- doped synthetic enstatites and defect geobarometry on natural orthopyroxenes from Earth's mantle. Eur J Mineral. 2012; 24:471–481.
25. Demouchy S. Diffusion of hydrogen in olivine grain boundaries and implications for the survival of water-rich zones in the Earth's mantle. Earth Planet Sci Lett. 2010; 295:305–313.
26. Brandon AD, Draper DS. Constraints on the oxidation state of mantle overlying subduction zones: An example from Simcoe, Washington, USA. Geochim Cosmochim Acta. 1996; 60:1739–1749.
27. Frost BR, Ballhaus C. Comment on "Constraints on the origin of the oxidation state of mantle overlying subduction zones: An example from Simcoe, Washington, USA" by A.D. Brandon and D.S. Draper. Geochim Cosmochim Acta. 1998; 62:329–331.
28. Brandon AD, Draper DS. Reply to the Comment by B.R. Frost and C. Ballhaus on Constraints on the origin of the oxidation state of mantle overlying subduction zones: An example from Simcoe, Washington, USA. Geochim Cosmochim Acta. 1998; 62:333–335.
29. Sambridge M, Fitz Gerald J, Kovács I, O'Neill HStC, Hermann J. Quantitative absorbance spectroscopy with unpolarized light: Part I. Physical and mathematical development. Am Mineral. 2008; 93:751–764.

30. Kovács I, Hermann J, O'Neill HStC, Fitz Gerald J, Sambridge M, Horváth G. Quantitative absorbance spectroscopy with unpolarized light: Part II. Experimental evaluation and development of a protocol for quantitative analysis of mineral IR spectra. Am Mineral. 2008; 93:765–778.
31. Jackson A, Parker RL, Sambridge M, Constable C, Wolf AS. The inverse problem of unpolarized infrared spectroscopy of geological materials: Estimation from noisy random sampling of a quadratic form. Am Mineral. 2018; 103:1176–1184.
32. Bell DR, Ihinger PD, Rossman GR. Quantitative analysis of trace OH in garnet and pyroxenes. Am Mineral. 1995; 80:465–474.

Europe PMC Funders Author Manuscripts

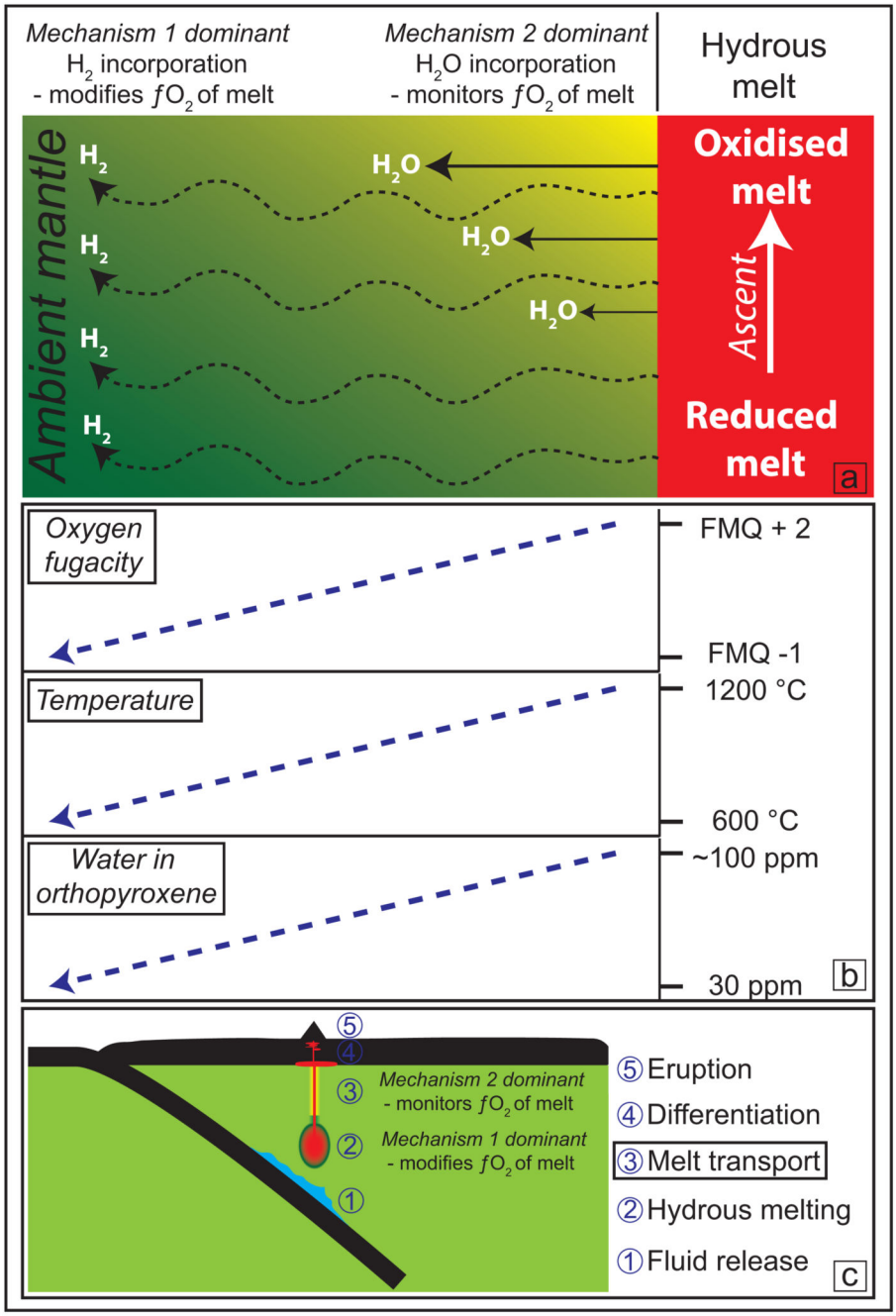

Fig. 1. Summary of the data and interpretations

a) Overview of the proposed geochemical model. An initially reduced melt is oxidised by H_2O dissociation and H_2 incorporation in the surrounding mantle (mechanism 1). As the progressively oxidised melt ascends, the mantle immediately adjacent to the melt channel is oxidised, resulting in the results shown in Fig. 2 and 3 (mechanism 2). b) Summary of how fO_2, T and H_2O in Ritter samples vary with distance from the melt channel. c) The key stages in arc magma generation and locations where mechanisms 1 and 2 dominate to modify and monitor melt fO_2 respectively.

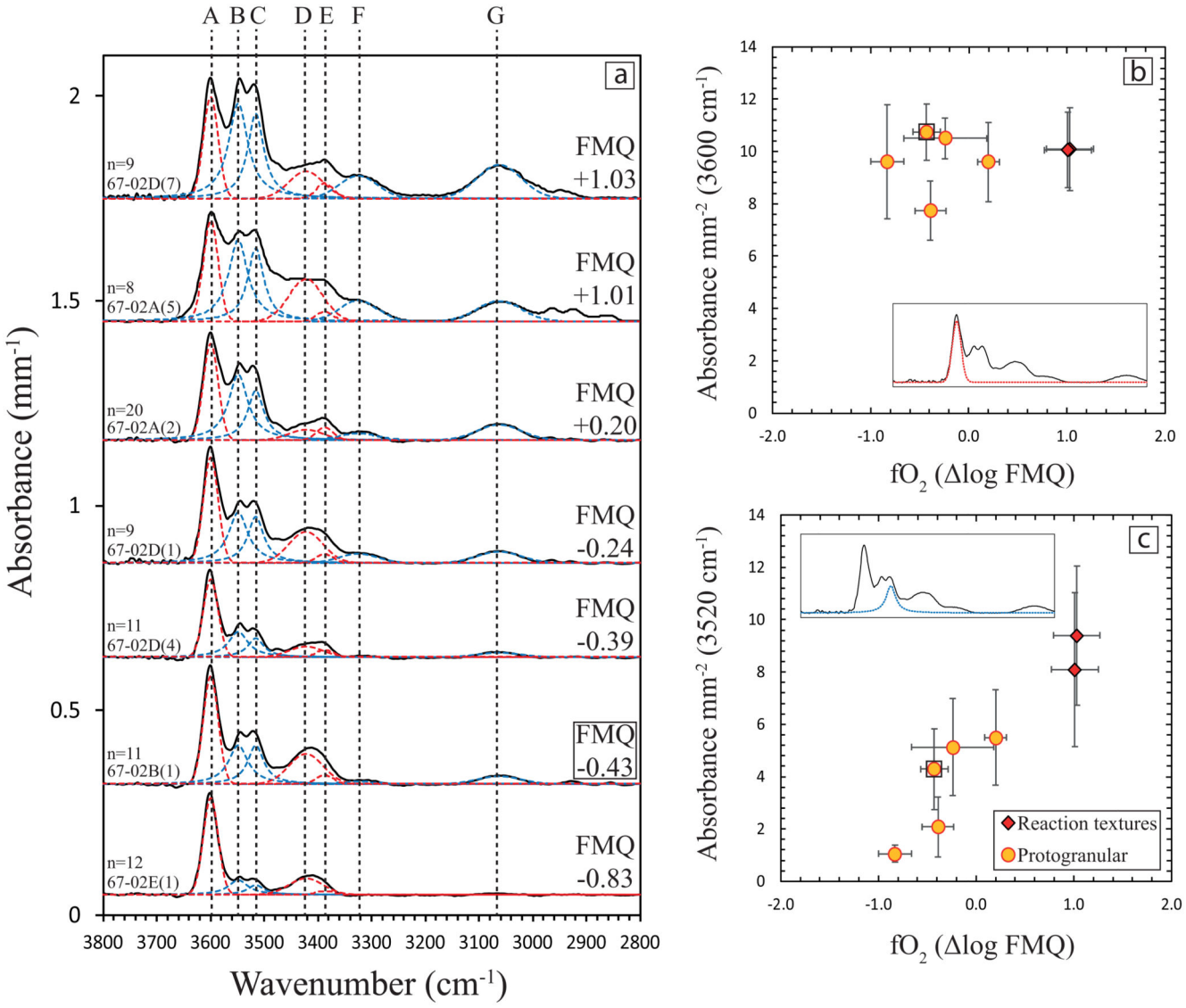

Fig. 2. Compilation of key FTIR data.

a) The average unpolarised infrared spectra from the cores of multiple randomly-oriented orthopyroxene from each sample (black curves). The spectra are baseline-corrected and arranged from most reduced (*bottom*) to most oxidised (*top*). Dashed curves represent deconvoluted bands whose intensities do (*blue*) and do not (*red*) correlate with fO_2. Band centres marked by vertical dashed lines are: A 3600 cm^{-1}, B 3544 cm^{-1}, C 3520 cm^{-1}, D 3420 cm^{-1}, E 3390 cm^{-1}, F 3325 cm^{-1}, G 3060 cm^{-1}. Subfigures b and c show examples of how redox-sensitive and redox-insensitive band absorbance varies with fO_2. Error bars represent 1σ of the mean. Sample names are consistent with previous studies[7,16,17].

Europe PMC Funders Author Manuscripts

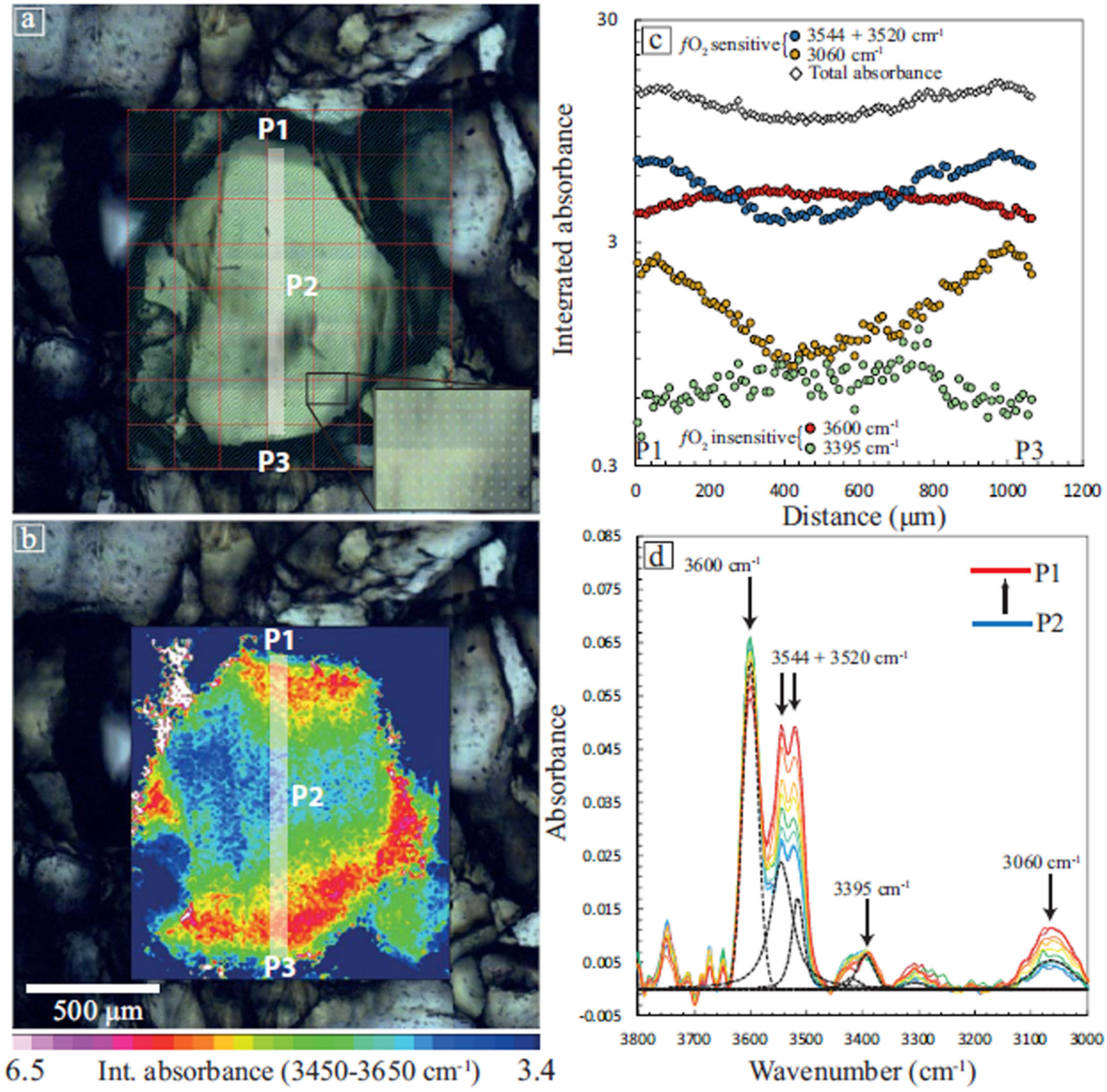

Fig. 3. An example of H_2O distribution in an orthopyroxene from sample 67-02B(1).

a) Arrangement of FPA detector mapping grids. The vertical white rectangle represents the extracted profile, with positions P1, P2 and P3 referred to in other sub-figures. b) Map showing the integrated absorbance of the dominant bands related to O-H stretching/ vibrations. c) Integrated absorbance of all contributing bands, and of individual bands which show either redox-sensitive or -insensitive behaviours, as a function of distance across the extracted profile. D) Evolution of infrared spectra from core (P2) to rim (P1) across the same profile.